Research Article | Vol. 29, No. 24 / 22 Nov 2021 / Optics Express 39766

Optics EXPRESS

Particle swarm optimization of SPM-enabled spectral selection to achieve an octave-spanning wavelength-shift

XINCAI DIAO,[1,2] RUNZHI CHEN,[1,2] AND GUOQING CHANG[1,2,3,*]

[1] *Beijing National Laboratory for Condensed Matter Physics, Institute of Physics, Chinese Academy of Sciences, Beijing 100190, China*
[2] *University of Chinese Academy of Sciences, Beijing 100049, China*
[3] *Songshan Lake Materials Laboratory, Dongguan, Guangdong 523808, China*
[*] *guoqing.chang@iphy.ac.cn*

Abstract: SPM-enabled spectral selection (SESS) constitutes a powerful fiber-optic technique to generate wavelength broadly tunable femtosecond pulses. In the current demonstration, the maximum tuning range is 400 nm and the energy conversion efficiency from the pump source to the outmost spectral lobes is ~25%. In this submission, we apply the particle swarm optimization method to the generalized nonlinear Schrödinger equation to identify the optimal parameters that maximize both the tuning range and the conversion efficiency. We show that SESS in an optical fiber with the optimized dispersion can deliver SESS pulses tunable in one octave wavelength range and the conversion efficiency can be as high as 80%. We further show the feasibility of experimental implementation based on specially designed fibers or on-chip waveguides.

1. Introduction

It is well known that propagation of energetic femtosecond pulses in optical fibers is accompanied by nonlinear effects such as self-phase modulation (SPM), self-steepening, and stimulated Raman scattering, which may substantially broaden the pulse spectrum [1]. This nonlinear spectral broadening process has resulted in several fiber-optic methods to generate wavelength tunable femtosecond pulses. These methods include dispersive-wave generation [2–5], fiber optical parametric oscillator/amplifier [6–8], supercontinuum generation (SCG) [9,10], soliton self-frequency shift (SSFS) [11–14], and SPM-enabled spectral selection (SESS) [15,16]. Limited by the phase-matching bandwidth mainly determined by optical fibers, tunable femtosecond sources based on dispersive-wave generation or fiber optical parametric oscillator/amplifier suffer from relatively narrow tuning range (<250 nm). SCG can generate octave-spanning spectrum and using a bandpass filter to select a spectral slice can produce femtosecond pulses after proper phase compensation. However, due to the intrinsic complicated phase associated with SCG process, phase compensation of the filtered spectrum demands complicated and lossy active devices. SSFS does not require post phase compensation and can directly deliver red-shifted transform-limited soliton pulses with large tuning range (>700 nm); unfortunately, the resulting pulses exhibit large timing-jitter noise and poor energy scalability [17]. As a recently developed wavelength-conversion method, SESS employs SPM-dominated spectral broadening to generate a broadened spectrum comprising well-isolated spectral lobes. Using proper optical filters to select the leftmost/rightmost spectral lobes produces nearly transform-limited femtosecond pulses with the center wavelength widely tunable. Unlike the well-known SSFS that produces center-wavelength red-shifted pulses, SESS generates pulses with the center wavelength either shorter or longer than that of the excited pulse. For example, we obtained ~100-fs pulses tunable from 825 nm to 1225 nm via SESS excited by 1.03-µm pulses [15]. As 1.55-µm pulses were used to excite SESS, we achieved ~100-fs pulses tunable in 1.3-1.7 µm [16]. These powerful

#442348 https://doi.org/10.1364/OE.442348
Journal © 2021 Received 2 Sep 2021; revised 28 Oct 2021; accepted 28 Oct 2021; published 15 Nov 2021

broadly tunable sources have been applied to multiphoton microscopy for biomedical imaging and protein crystal detection [18–20]. To date, the maximum wavelength tuning range offered by SESS is 400 nm, and the conversion efficiency from the pump source to the leftmost/rightmost spectral lobes is ~25%. A question naturally rises: can we further increase both the tuning range and the conversion efficiency? In this paper, we apply particle swarm optimization (PSO) method to the generalized nonlinear Schrödinger equation (GNLSE) to explore the optimal parameters for implementing broadly tunable and highly efficient SESS sources. We show that an optimized fiber dispersion allows generation of SESS pulses with the wavelength tunability exceeding one octave and the conversion efficiency reaching >80%.

2. PSO applied to GNLSE for modelling SESS

The propagation of a femtosecond pulse in an optical fiber can be accurately modeled by the well-known GNLSE [1]:

$$\begin{aligned}\frac{\partial A(z,T)}{\partial z} &- \left(\sum_{n\geq 2}\beta_n \frac{i^{n+1}}{n!}\frac{\partial^n}{\partial T^n}\right)A(z,T)\\ &= i\gamma\left(1+\frac{i}{\omega_0}\frac{\partial}{\partial T}\right)\\ &\times\left(A(z,T)\int_{-\infty}^{+\infty}R(t')\mid A(z,T-t')\mid^2 dt'\right),\end{aligned} \tag{1}$$

where $A(z, T)$ is the amplitude envelope of the temporal pulse at position z. β_n denotes the nth-order dispersion coefficient. γ is the nonlinear parameter defined by $\gamma = (\omega_0 n_2)/(cA_{eff})$, where ω_0 is the center frequency, n_2 is the nonlinear index coefficient, c is the light speed in vacuum, and A_{eff} is the mode-field area. $R(t)$ denotes the nonlinear response function, which can be written as

$$R(t) = (1-f_R)\,\delta(t) + f_R\frac{\tau_1^2+\tau_2^2}{\tau_1\tau_2^2}exp\left(\frac{-t}{\tau_2}\right)sin\left(\frac{t}{\tau_1}\right), \tag{2}$$

where f_R represents the fractional contribution of the delayed Raman response to nonlinear polarization and takes the typical value of 0.18. τ_1 and τ_2 are two parameters to fit well to the Raman-gain spectrum, which take the value of 12.2 fs and 32 fs, respectively.

Although SESS relies on SPM-dominated spectral broadening, fiber dispersion plays an increasingly important role as we try to shift the leftmost/rightmost spectral lobes further away. In Ref. [21], we simulated propagation of femtosecond pulses in three fibers with positive, zero, and negative group-velocity dispersion (GVD), respectively, and the purpose was to show that SESS can be achieved in fibers with arbitrary sign of GVD.

To further show that the fiber GVD also determines the wavelength tuning range and energy conversion efficiency, we here simulate propagation of 100-nJ, 200-fs Gaussian pulse in three fibers with their GVD set at 10 fs^2/mm, 0, and −10 fs^2/mm, respectively. For simplicity, higher-order dispersions are neglected. All the fibers have a mode-field diameter (MFD) of 7 µm. Figure 1(a, b, c) depict the spectral evolution in these three fibers with a length up to 2 cm. For all three cases, the propagation is accompanied by rapid spectral broadening and the resulting spectra consist of several spectral lobes. To have a better comparison, we plot in Fig. 1(d-f) the spectra at the output of 2-cm fibers. The leftmost (rightmost) spectral lobe of the output spectrum from the fiber with 0-fs^2/mm GVD contains 22% (35%) of the total input energy [Fig. 1(e)]. The result in Fig. 1(d) shows that the resulting spectrum becomes narrower and spectral lobes tend to wash out as positive GVD exists; the leftmost (rightmost) spectral lobe contains 22% (31%) of total input energy. For the fiber with negative GVD, soliton compression

Optics EXPRESS

occurs and the associated larger nonlinear phase shift results in a broader spectrum [Fig. 1(f)]. The leftmost (rightmost) spectral lobe peaks at 1.22 µm (1.75 µm) containing 7% (53%) of total input energy. The SESS pulses generated by filtering the leftmost (rightmost) spectral lobe of the spectra in Fig. 1(d-f) are shown as the black (red) curves in Fig. 1(g-i). These pulses have a duration varying between 38 fs and 105 fs. Also plotted in these figures are the corresponding transform-limited pulses (dashed lines). Although the fiber dispersion affects the duration and energy of these SESS pulses, they are all close to be transform-limited.

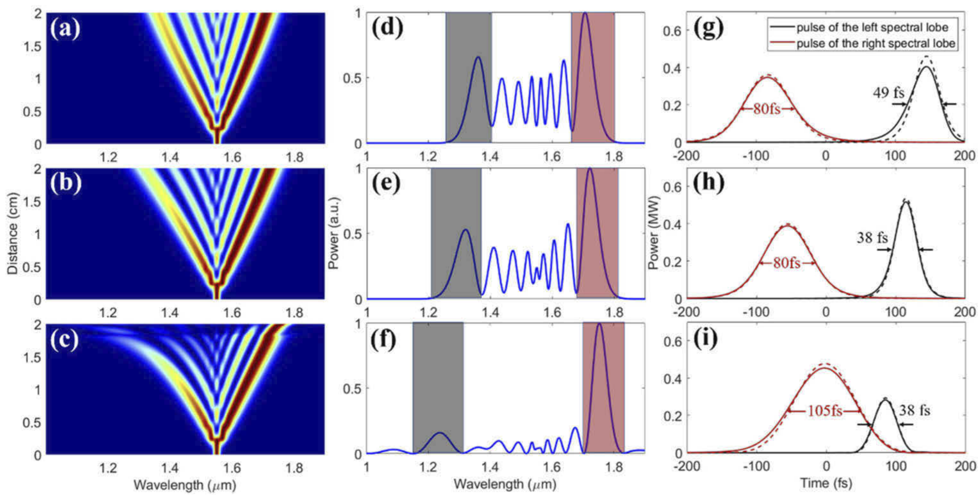

Fig. 1. Simulation results of the optical spectral evolution (a-c), output spectra (d-f), and filtered SESS pulses (g-i) for a 100-nJ, 200-fs pulse centered at 1.55 µm propagating in 2-cm optical fibers with 7-µm MFD and different GVD at 1.55 µm: 10 fs^2/mm for (a, d, g), 0 fs^2/mm for (b, e, h), and -10 fs^2/mm for (c, f, i). The shaded areas in (d, e, f) mark the leftmost and the rightmost spectral lobes in (a, b, c), respectively. Solid-lines in (g, h, i) show the SESS pulses and dashed lines represent the corresponding transform-limited pulses.

The results in Fig. 1 clearly indicate that, in addition to nonlinearity, fiber dispersion is crucial to determine the wavelength tuning range and the energy conversion efficiency. To explore the full potential of SESS for effectively generating broadly tunable pulses, we employ PSO method to optimize the fiber parameters. As a stochastic population-based algorithm, PSO was introduced by Kennedy and Eberhart in 1995 [22] and soon was widely used to optimize the nonlinear and non-continual problems in different research fields [23–25]. Several groups have applied PSO to optimize optical nano-antennas, optical fiber systems involving stimulated Raman scattering or stimulated Brillouin scattering, and mode-locked fiber lasers [26–29]. Compared with the well-known genetic algorithm that is widely adopted in optics, PSO has only one operator (velocity calculation) while genetic algorithm needs three (selection, crossover, and mutation), which makes PSO relatively easy to implement. Additionally, the global best particle and the inertia term in PSO avoid the convergence to a local optimum.

PSO was inspired by the behavior of the bird swarm. To locate the position of the food, birds in a swarm learn from their experience and share information, which correspond to the cognitive and social mechanism of the PSO algorithm. Figure 2 illustrates the iteration flowchart of PSO algorithm. Two D-dimensional vector $X_i = (X_{i1}, \ X_{i2}, \ \ldots, \ X_{iD})$ and $V_i = (V_{i1}, \ V_{i2}, \ \ldots, \ V_{iD})$ are randomly generated to represent the position and velocity of the i^{th} particle, respectively. The position vector X_i is substituted into an objective function to produce a fitness value representing the fitness of X_i. For the i^{th} particle, the optimal position of its own historical position is recorded as personal best $P_i = (P_{i1}, \ P_{i2}, \ \ldots, \ P_{iD})$ and the optimal position of all particles is recorded

Optics EXPRESS

as global best $P_g = (P_{g1}, \ P_{g2}, \ \ldots, \ P_{gD})$. The velocity of the i^{th} particle at the t^{th} iteration $V_i(t+1)$, which denotes the difference between $X_i(\mathrm{t}+1)$ and $X_i(\mathrm{t})$, gives the form as

$$\vec{V}_i(t+1) = w{*}\vec{V}_i(t) + c_1 r_1(\vec{P}_i(t) - \vec{X}_i(t)) + c_2 r_2(\vec{P}_g(t) - \vec{X}_i(t)) \tag{3}$$

$$\vec{X}_i(t+1) = \vec{X}_i(t) + \vec{V}_i(t+1) \tag{4}$$

where t denotes the iteration of the particle swarm. w is the inertia weight factor. The acceleration constants c_1 and c_2 affect the contribution of P_i and P_g, respectively. They are usually set between 1.5 and 2.5 to improve the convergence performance of the algorithm. Two random functions r_1 and r_2 are distributed between 0 and 1.

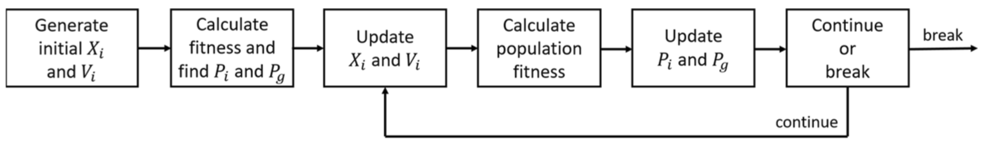

Fig. 2. Flowchart of PSO algorithm.

3. Single-objective optimization for SESS

In our optimization, we randomly generate an initial swarm with a few particles. Each particle corresponds to a 5-dimensional vector X_i, which represents a group of parameters with 5 variables, i.e., fiber length L, MFD, β_2, β_3, and β_4. A 200-fs Gaussian pulse centered at 1.55 µm with 150-nJ energy is injected into these fibers. Nonlinear propagation of the pulse in the fibers is modeled by the GNLSE [i.e., Eq. (1)]. Two windows are pre-set at both sides of the pump wavelength. Once the peak of a spectral lobe appears in the windows, the entire spectral lobe is selected. The Fourier transform of each individual side lobe represents the corresponding temporal pulse, and the transform-limited pulse can also be calculated by eliminating the spectral phase. In our SESS optimization, we define a fitness function as

$$\mathit{fitness} = \eta_1 \times \eta_2. \tag{5}$$

$$\eta_1 = \frac{E_l + E_r}{E_{in}} \tag{6}$$

$$\eta_2 = \frac{SR_l + SR_r}{2} \tag{7}$$

E_l (E_r) represents the energy contained in the leftmost (rightmost) spectral lobe, and E_{in} is the input energy. η_1 denotes the energy conversion efficiency. SR_l (SR_r) is the strehl ratio of the SESS pulse corresponding to the leftmost (rightmost) spectral lobe, which is the ratio between the peak power of filtered SESS pulse and the transform-limited pulse. Indeed η_2 quantifies the SESS pulse quality. The simulation parameters are chosen as follows:

1) The inertia factor w is set to linearly decrease from 0.8 to 0.3 through the whole iteration process, and the cognitive factor c_1 and social factor c_2 are set at 1.5 and 2.5, respectively.

2) A maximum step number of 400 is set to avoid an overlong calculation time. The fitness value returns to zero if the maximum step value is reached.

3) We first set the search range at 1-5 cm for fiber length, 2-20 µm for MFD, -100-100 fs^2/mm for β_2, -200-200 fs^3/mm for β_3, and -1000-1000 fs^4/mm for β_4. The PSO algorithm running with 300 particles and 300 iterations shows great convergence. The computation time is

Optics EXPRESS

about 2 hours using a common laptop. After several trials, we can substantially reduce the computation time by searching in a smaller parameter space: 1.5-3.5 cm for fiber length, 4-12 µm for MFD, -10-0 fs^2/mm for β_2, 0-200 fs^3/mm for β_3, and 0-1000 fs^4/mm for β_4. Furthermore, a reflection mechanism is introduced to reset the particles into the search range if they stray out.

To investigate the effects of dispersion, we perform the optimization for two cases: (1) optimizing β_2 and β_3, and (2) optimizing β_2, β_3, and β_4.

3.1. Optimization of β_2 and β_3

In this section, only the fiber length, MFD, the 2$^{\text{nd}}$- and the 3$^{\text{rd}}$- order dispersion are considered. To show the astringency of the algorithm, we run the PSO with 300 particles and 300 iterations with the pass bands of the filter pre-set at 1.2 µm and 1.8 µm with 60-nm bandwidth. Figure 3 plots the mean fitness value (blue triangle) and global best fitness value (red circle) as a function of iteration. As the iteration number increases, the global best fitness reaches a constant of 0.705 after 100 iterations, and the mean fitness gradually converges to the global best fitness, which demonstrates the astringency of the PSO algorithm.

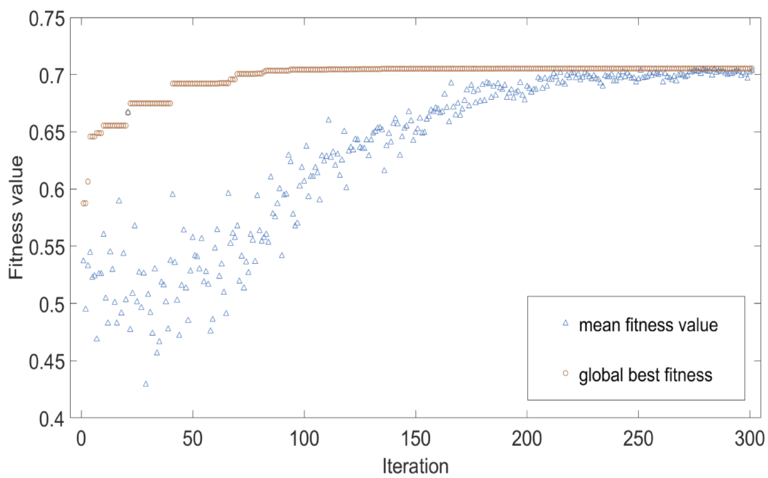

Fig. 3. Best fitness and mean fitness as a function of iteration.

The global best particle (red circle) after 100 iteration corresponds to the optimized fiber parameters such as fiber length, MFD, β_2, and β_3, which, in this optimization, are 3.2 cm, 10.5 µm, -6.2 fs^2/mm, and 21.7 fs^3/mm, respectively. Figure 4(a) and (b) depict the spectrum and pulse evolution along with the increased propagation distance. The white dashed line in Fig. 4(a) indicates the zero-dispersion wavelength (ZDW) of the fiber, which is 1.25 µm. The output spectrum after the fiber [Fig. 4(c)] comprises well-isolated spectral lobes. Due to the anomalous dispersion at the center wavelength, the pulse is compressed along the fiber without soliton fission [inset of Fig. 4(c)]. The 3-dB bandwidth of the selected leftmost (rightmost) spectral lobe is 147 nm (131 nm) and the corresponded temporal pulse FWHM is 34 fs (87 fs) with 40-nJ (70-nJ) pulse energy [solid lines in Fig. 4(d)]. The total energy conversion efficiency is 73%. The dashed lines in Fig. 4(d) represent the corresponding transform-limited pulses, and clearly the resulting SESS pulse are nearly transform-limited.

Optics EXPRESS

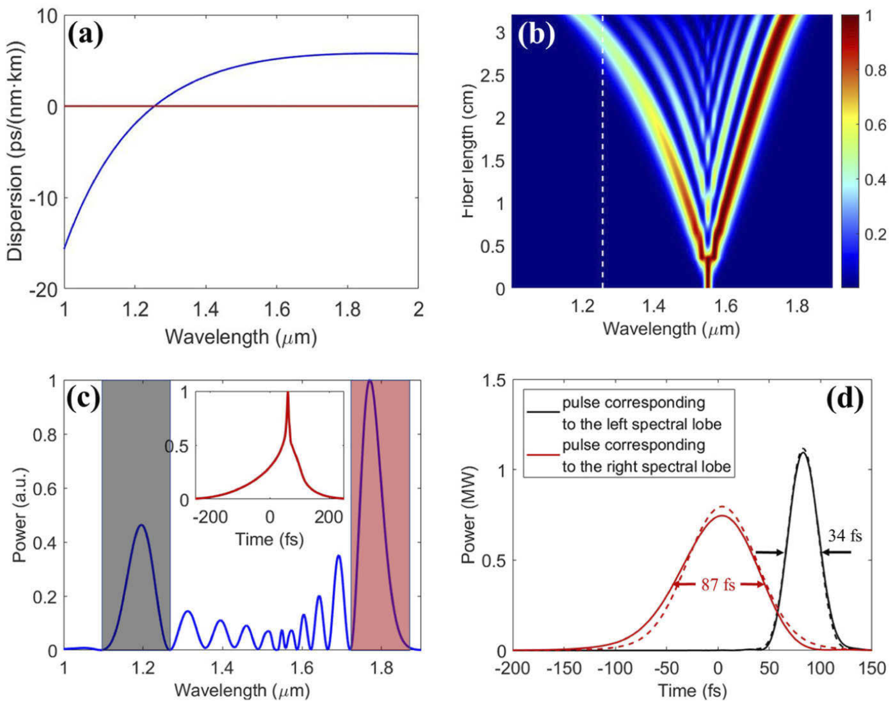

Fig. 4. SESS results given by PSO of fiber length, MFD, β_2, and β_3. (a) Dispersion of the optimized fiber. (b) Spectral evolution along with fiber distance. The white dash line marks the zero-dispersion wavelength. (c) Spectrum at the output of 3.2-cm fiber. Inset: pulse at the output. (d) SESS pulses corresponding to the leftmost spectral lobe (black solid line) and the rightmost spectral lobe (red solid line). Dashed lines show the corresponding transform-limited pulses.

3.2. Optimization of β_2, β_3, and β_4

In Section 3.1, we only consider β_2 and β_3, and therefore the fiber dispersion has only one ZDW. Nowadays, the rapidly developed photonic crystal fibers (PCFs) or on-chip waveguides provide more degrees of freedom to engineer the fiber parameters. For instance, by adjusting the fiber pitch, PCFs with two or three ZDWs can be achieved. PCFs with two ZDWs are suitable for supercontinuum generation with the pump wavelength located between the two ZDWs [30,31]. These fibers exhibit a relatively large β_4. In this section, we include β_4 in the optimization of fiber dispersion. The passbands of the filter are set at 1.2 μm and 1.8 μm with 60-nm bandwidth to select the leftmost/rightmost spectral lobes. After running the PSO algorithm with 100 particles and 100 iterations, the optimized results for fiber length, MFD, β_2, β_3, and β_4 are 2.3 cm, 8.2 μm, -7.7 fs^2/mm, 0.4 fs^3/mm, and 934 fs^4/mm, respectively.

Figure 5(a) plots the fiber dispersion with two ZDWs located at 1.4 μm and 1.73 μm. Figure 5(b) illustrates the spectral evolution along the fiber length, and the two dashed lines mark the ZDWs. As the pulse propagates from 0 cm to 1.5 cm, the spectrum broadens symmetrically by SPM until the outmost spectral lobes start to shift into the normal dispersion region. For further propagation, the spectral lobes in the central spectral region fade away and more energy transfers to the two outmost spectral lobes. This spectral evolution can be explained as a non-degenerate four-wave mixing process: the phase-matching between the spectral lobes in the central region and the two outmost spectral lobes causes the energy conversion [30]. Figure 5(c) shows that, after propagation of 2.3 cm, the two spectral lobes peak at 1.23 μm and 1.79 μm, respectively; the

Optics EXPRESS

inset shows the corresponding pulse. Figure 5(d) plots the SESS pulses: the leftmost (rightmost) spectral lobe has an energy of 54 nJ (69 nJ) with 60-fs (107-fs) pulse FWHM. Given 150-nJ input energy, these two lobes include 82% of the energy. For a comparison, the dashed lines represent the transform-limited pulses. Apparently the two SESS pulses are nearly transform-limited.

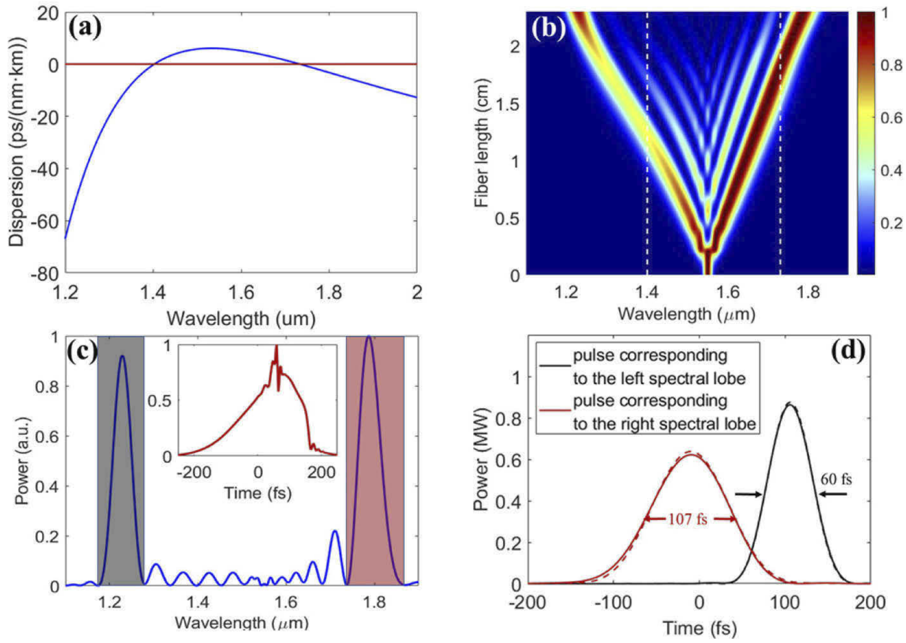

Fig. 5. SESS results given by PSO of fiber length, MFD, β_2, β_3, and β_4. (a) GVD of the optimized fiber. (b) Spectral evolution. Two white dashed lines mark the two ZDWs. (c) Broadened spectrum after propagating 2.3 cm with the pulse shown as inset. (d) SESS pulses corresponding to the leftmost spectral lobe (black solid line) and the rightmost spectral lobe (red solid line). Dashed lines show the corresponding transform-limited pulses.

4. Multi-objective PSO

Problems with two or more objectives (e.g., large spectral tuning range and high energy conversion efficiency) need more complicated fitness function to guide the particles toward the optimal solution. This improved algorithm is known as multi-objective PSO. In this section, we introduce a multi-objective fitness function to simultaneously optimize both the conversion efficiency and the wavelength separation between the leftmost and rightmost spectral lobes, which takes the form

$$fitness = \frac{E_l + E_r}{E_{in}} \times \frac{SR_l + SR_r}{2} + \frac{(\lambda_{max} - \lambda_{min})}{\lambda_0} \tag{8}$$

The first term on the right-hand side represents the energy conversion efficiency of these two side lobes and the second item denotes the wavelength separation between the left and right lobe, which is normalized to λ_0 (is set at 1.55 µm in this simulation).

After running the PSO algorithm with 200 particles and 200 iterations, the optimized results for fiber length, MFD, β_2, β_3, and β_4 are 1.73 cm, 5.8 µm, -8.5 fs^2/mm, 24.1 fs^3/mm, and 0.0012 fs^4/mm, respectively. The output results are summarized in Fig. 6. The dispersion curve of the optimized fiber has a ZDW at 1.2 µm [blue curve in Fig. 6(a)]. For comparison, we also plot the dispersion of a PM980 fiber [black curve in Fig. 6(a)]. The spectral evolution in Fig. 6(b) is similar with that in Fig. 5(b) but exhibits a much larger wavelength coverage (the white dashed line makes the ZDW). Figure 6(c) shows the output spectrum after propagating 1.73 cm. The leftmost and rightmost spectral lobes peak at 0.91 µm and 1.92 µm, respectively, resulting in a wavelength tuning range exceeding one octave. The leftmost (rightmost) spectral lobe has energy of 40 nJ (68 nJ), corresponding to 72% conversion efficiency. The red (black) solid curve in Fig. 6(d) shows the 94-fs (33-fs) pulse corresponding to the filtered rightmost (leftmost) spectral lobe.

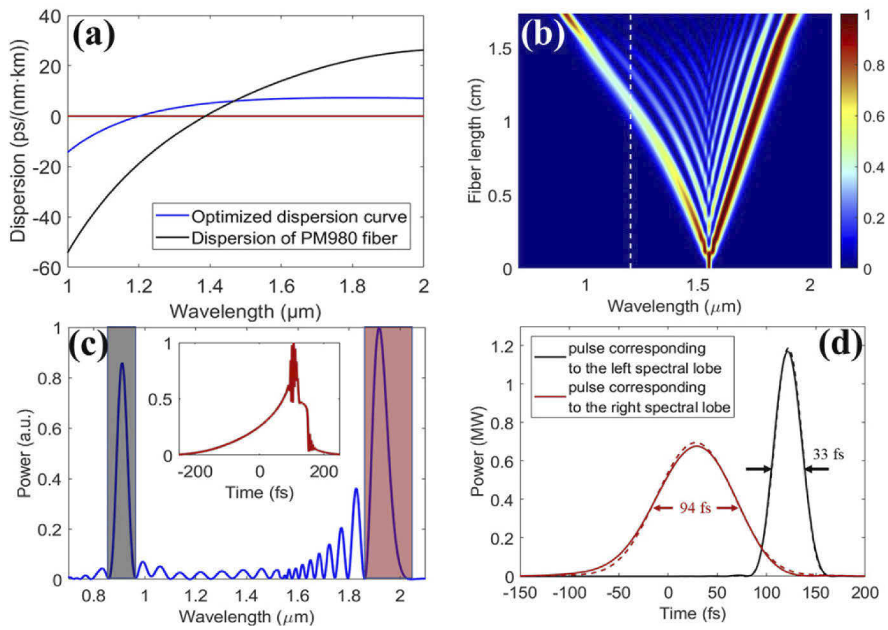

Fig. 6. Joint optimization of conversion efficiency and wavelength tuning range. (a) GVD of optimized fiber and PM980 fiber. (b) Spectral evolution. (c) Broadened spectrum after propagating 1.73 cm with the pulse shown as inset. (d) SESS pulses corresponding to the leftmost spectral lobe (black solid line) and the rightmost spectral lobe (red solid line). Dashed lines show the corresponding transform-limited pulses.

Compared with the results in Section 3.2, the multi-objective PSO leads to a larger wavelength tuning range (1.01 µm versus 0.56 µm) and a less conversion efficiency (72% versus 82%). As expected from Eq. (8), a trade-off exists between the tuning range and the conversion efficiency. Changing the relative weight between the two terms in Eq. (8) can generate the optimized results more in favor of tuning range (or conversion efficiency).

5. Possible experimental implementation

The PSO results indicate that optical fibers with properly tailored dispersion can produce SESS pulses with high conversion efficiency as well as large tuning range. Since these dispersion curves are predicted by PSO algorithm, one might raise the question whether they are feasible experimentally. To answer this question, we consider SESS in a numerically designed PCF in with two ZDWs at 1129 nm and 1637 nm [black curve in Fig. 7(a)] [32]. The black curve in Fig. 8(b) shows the broadened spectrum for a 150-nJ 200-fs Gaussian pulse centered at 1500 nm propagating 3.5 mm in this PCF. The leftmost (rightmost) spectral lobe peaks at 936 nm (1744 nm) and contains 30 nJ (77 nJ) energy. This corresponds to 71% of energy conversion efficiency. It is noteworthy that experimentally preparing a PCF as short as 3.5 mm and coupling light into it is possible. In our previous experimental work, we successfully demonstrated nonlinear wavelength conversion in a 2-mm long PCF [3].

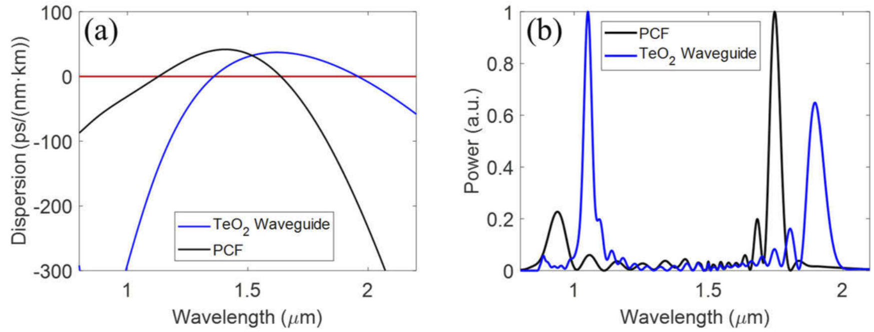

Fig. 7. (a) Dispersion of PCF (black curve) and TeO_2 waveguide (blue curve). (b) Output spectrum of a 150-nJ, 200-fs Gaussian pulse propagating in the PCF (black curve) and a 15-nJ 200-fs Gaussian pulse propagating in 3-mm TeO_2 waveguide (blue curve).

Besides optical fibers, on-chip waveguides constitute another important platform for nonlinear optical wavelength conversion. The waveguide structure can be precisely engineered to achieve a varied waveguide dispersion along the direction of propagation to produce a desired spectrum [33]. The propagation of ultrafast pulse in the waveguide is also described by the GNLSE despite that the nonlinear coefficient n_2 of the waveguide is significantly larger than that of the silica fiber. The blue curve in Fig. 7(a) shows the dispersion curve of a TeO_2 waveguide [34]. The blue curve in Fig. 7(b) corresponds to the output spectrum of a 15-nJ, 200-fs Gaussian pulse after propagating 3-mm in this waveguide. With two ZDWs located at 1358 nm and 1960 nm, the two spectral lobes are extended to 1050 nm and 1900 nm with an energy of 5.1 nJ and 6 nJ, respectively, corresponding to 74% energy conversion efficiency.

6. Conclusion

In conclusion, we apply the PSO algorithm to the GNLSE to optimize an optical waveguide such that the resulting SESS pulses feature both large tuning range and high conversion efficiency. Using single-objective PSO to maximize the energy conversion efficiency, we show that an optical fiber with two ZDWs can deliver tens-of-nanojoule transform-limited SESS pulses with the conversion efficiency as high as 82%. Multi-objective PSO allows a joint optimization of tuning range and conversion efficiency, and the resulting SESS pulses can be tuned within the wavelength range of 0.91-1.92 µm, which exceeds one octave. A comparison between single- and multi- objective optimizations reveals a trade-off between the tuning range and the conversion efficiency. We also discuss the feasibility of experimental implementation based on customized fibers or TeO_2 waveguides, both of which have two ZDWs. Ongoing work is to experimentally demonstrate such broadly tunable energetic SESS sources, which will find important applications in multiphoton microscopy and generation of high-power long-wave mid-infrared femtosecond pulses [35,36].

Apart from SESS, the PSO algorithm can be applied to optimize other nonlinear processes that are sensitive to the dispersion. For example, the PSO algorithm can be used to supercontinuum generation to optimize both the bandwidth and flatness. It can also optimize soliton self-frequency shift to maximize the energy and the wavelength shift of a Raman soliton. We anticipate that the PSO algorithm will become a powerful optimization tool for nonlinear waveguide optics.

Funding. Key-Area Research and Development Program of Guangdong Province (2018B090904003); National Natural Science Foundation of China (11774234); Chinese Academy of Sciences (YJKYYQ20190034).

Optics EXPRESS

Acknowledgment. We thank Professor Zhiyi Wei and Dr. Ergun Simsek for useful discussions.

Disclosures. The authors declare no conflicts of interest.

Data availability. Data underlying the results presented in this paper are not publicly available at this time but may be obtained from the authors upon reasonable request.

References

1. G. P. Agrawal, *Nonlinear Fiber Optics*, 5th ed. (Elsevier, 2013).
2. F. Tauser, F. Adler, and A. Leitenstorfer, "Widely tunable sub-30-fs pulses from a compact erbium-doped fiber source," Opt. Lett. **29**(5), 516–518 (2004).
3. G. Q. Chang, L. J. Chen, and F. X. Kärtner, "Highly efficient Cherenkov radiation in photonic crystal fibers for broadband visible wavelength generation," Opt. Lett. **35**(14), 2361–2363 (2010).
4. H. Tu, J. Laegsgaard, R. Zhang, S. Tong, Y. Liu, and S. A. Boppart, "Bright broadband coherent fiber sources emitting strongly blue-shifted resonant dispersive wave pulses," Opt. Express **21**(20), 23188–23196 (2013).
5. K. C. Li, L. H. Huang, J. H. Liang, and M. C. Chan, "Simple approach to three-color two-photon microscopy by a fiber-optic wavelength convertor," Biomed. Opt. Express **7**(11), 4803–4815 (2016).
6. T. Gottschall, T. Meyer, M. Schmitt, J. Popp, J. Limpert, and A. Tünnermann, "Four-wave-mixing-based optical parametric oscillator delivering energetic, tunable, chirped femtosecond pulses for non-linear biomedical applications," Opt. Express **23**(18), 23968–23977 (2015).
7. K. Yang, J. Jiang, Z. Guo, Q. Hao, and H. Zeng, "Tunable Femtosecond Laser from 965 to 1025 nm in Fiber Optical Parametric Oscillator," IEEE Photonics Technol. Lett. **30**(7), 607–610 (2018).
8. M. Brinkmann, A. Fast, T. Hellwig, I. Pence, C. L. Evans, and C. Fallnich, "Portable all-fiber dual-output widely tunable light source for coherent Raman imaging," Biomed. Opt. Express **10**(9), 4437–4449 (2019).
9. Y. Liu, H. Tu, W. A. Benalcazar, E. J. Chaney, and S. A. Boppart, "Multimodal nonlinear microscopy by shaping a fiber supercontinuum from 900 to 1160 nm," IEEE J. Sel. Top. Quantum Electron. **18**(3), 1209–1214 (2012).
10. H. Tu, Y. Liu, D. Turchinovich, M. Marjanovic, J. K. Lyngsø, J. Lægsgaard, E. J. Chaney, Y. Zhao, S. You, W. L. Wilson, B. Xu, M. Dantus, and S. A. Boppart, "Stain-free histopathology by programmable supercontinuum pulses," Nat. Photonics **10**(8), 534–540 (2016).
11. K. Wang and C. Xu, "Tunable high-energy soliton pulse generation from a large-mode-area fiber and its application to third harmonic generation microscopy," Appl. Phys. Lett. **99**(7), 071112 (2011).
12. Y. Tang, L. G. Wright, K. Charan, T. Wang, C. Xu, and F. W. Wise, "Generation of intense 100 fs solitons tunable from 2 to 4.3 µm in fluoride fiber," Optica **3**(9), 948–951 (2016).
13. J. W. Nicholson, A. Desantolo, W. Kaenders, and A. Zach, "Self-frequency-shifted solitons in a polarization maintaining, very-large-mode area, Er-doped fiber amplifier," Opt. Express **24**(20), 23396–23402 (2016).
14. L. Rishøj, B. Tai, P. Kristensen, and S. Ramachandran, "Soliton self-mode conversion: revisiting Raman scattering of ultrashort pulses," Optica **6**(3), 304–308 (2019).
15. W. Liu, C. Li, Z. G. Zhang, F. X. Kärtner, and G. Q. Chang, "Self-phase modulation enabled, wavelength-tunable ultrafast fiber laser sources: an energy scalable approach," Opt. Express **24**(14), 15328–15340 (2016).
16. H. Y. Chung, W. Liu, Q. Cao, F. X. Kärtner, and G. Q. Chang, "Er-fiber laser based, energy scalable ultrafast sources tunable in 1300-1700 nm," Opt. Express **25**(14), 15760 (2017).
17. G. Zhou, M. Xin, F. X. Kärtner, and G. Q. Chang, "Timing jitter of Raman solitons," Opt. Lett. **40**(21), 5105–5108 (2015).
18. H. Y. Chung, R. Greinert, F. X. Kärtner, and G. Q. Chang, "Multimodal imaging platform for optical virtual skin biopsy enabled by a fiber-based two-color ultrafast laser source," Biomed. Opt. Express **10**(2), 514–525 (2019).
19. H. Y. Chung, W. Liu, Q. Cao, R. Greinert, F. X. Kärtner, and G. Q. Chang, "Novel fiber-based ultrafast source tunable between 1.15 µm and 1.35 µm for harmonic generation microscopy in human skin," IEEE J. Sel. Top. Quantum Electron. **25**(1), 1 (2018).
20. Q. D. Cheng, H. Y. Chung, R. Schubert, S. H. Chia, S. Falke, C. N. Mudogo, F. X. Kärtner, G. Q. Chang, and C. Betzel, "Protein-crystal detection with a compact multimodal multiphoton microscope," Commun. Biol. **3**(1), 569 (2020).
21. H. Y. Chung, W. Liu, Q. Cao, L. W. Song, F. X. Kärtner, and G. Q. Chang, "Megawatt peak power tunable femtosecond source based on self-phase modulation enabled spectral selection," Opt. Express **26**(3), 3684–3695 (2018).
22. J. Kennedy and R. Eberhart, "Particle swarm optimization," *Proceedings of ICNN'95 - International Conference on Neural Networks* **4**, 1942–1948 (1995).
23. J. Salerno, "Using the particle swarm optimization technique to train a recurrent neural model," *Proceedings Ninth IEEE International Conference on Tools with Artificial Intelligence*, (45–49) 1997.
24. J. Kennedy and W. M. Spears, "Matching algorithms to problems: an experimental test of the particle swarm and some genetic algorithms on the multimodal problem generator," *1998 IEEE International Conference on Evolutionary Computation Proceedings. IEEE World Congress on Computational Intelligence (Cat. No.98TH8360)*, 78–83 (1998).
25. S. Naka, T. Genji, T. Yura, Y. Fukuyama, and N. Hayashi, "Distribution state estimation considering nonlinear characteristics of practical equipment using hybrid particle swarm optimization," *PowerCon 2000. 2000 International Conference on Power System Technology. Proceedings (Cat. No.00EX409)* **2**, 1083–1088 (2000).

Optics EXPRESS

26. H. M. Jiang, K. Xie, and Y. F. Wang, "Shooting algorithm and particle swarm optimization based Raman fiber amplifiers gain spectra design," Opt. Commun. **283**(17), 3348–3352 (2010).
27. L. Lobachinsky and A. Bahabad, "Using Particle Swarm Optimization to Design Broadband Optical Nano-antennas for Nonlinear Optics," *Frontiers in Optics 2014*, OSA Technical Digest (online) (Optical Society of America, 2014), paper FTh4E.3.
28. H. A. Al-Asadi, M. H. Al-Mansoori, S. Hitam, M. I. Saripan, and M. A. Mahdi, "Particle swarm optimization on threshold exponential gain of stimulated Brillouin scattering in single mode fibers," Opt. Express **19**(3), 1842–1853 (2011).
29. A. Kokhanovskiy, E. Kuprikov, A. Bednyakova, I. Popkov, S. Smirnov, and S. Turitsyn, "Inverse design of mode-locked fiber laser by particle swarm optimization algorithm," Sci. Rep. **11**(1), 13555 (2021).
30. K. M. Hilligsøe, T. V. Andersen, H. N. Paulsen, C. K. Nielsen, K. Mølmer, S. Keiding, R. Kristiansen, K. P. Hansen, and J. J. Larsen, "Supercontinuum generation in a photonic crystal fiber with two zero dispersion wavelengths," Opt. Express **12**(6), 1045–1054 (2004).
31. P. Falk, M. H. Frosz, and O. Bang, "Supercontinuum generation in a photonic crystal fiber with two zero-dispersion wavelengths tapered to normal dispersion at all wavelengths," Opt. Express **13**(19), 7535–7540 (2005).
32. E. Wang, P. Cheng, W. Zhao, J. Li, and X. Zhou, "Photonic crystal fibers with high birefringence and multiple zero dispersion wavelengths," Opt. Fiber Technol. **58**, 102309 (2020).
33. C. Ciret and S. P. Gorza, "Generation of ultra-broadband coherent supercontinua in tapered and dispersion-managed silicon nanophotonic waveguides," J. Opt. Soc. Am. B **34**(6), 1156–1162 (2017).
34. N. Singh, H. M. Mbonde, H. C. Frankis, E. Ippen, and F. X. Kärtner, "Nonlinear silicon photonics on CMOS compatible tellurium oxide," Photonics Res. **8**(12), 1904 (2020).
35. Q. Cao, F. X. Kärtner, and G. Q. Chang, "Towards high power longwave mid-IR frequency combs: power scalability of high repetition-rate difference-frequency generation," Opt. Express **28**(2), 1369 (2020).
36. G. J. Zhou, Q. Cao, F. X. Kärtner, and G. Q. Chang, "Energy scalable, offset-free ultrafast mid-IR source harnessing self-phase modulation spectral selection," Opt. Lett. **43**(12), 2953 (2018).